Pressure Induced Isostructural Metastable Phase Transition of Ammonium Nitrate

ARTICLE *in* THE JOURNAL OF PHYSICAL CHEMISTRY A · SEPTEMBER 2011

Impact Factor: 2.69 · DOI: 10.1021/jp207754z · Source: PubMed

THE JOURNAL OF PHYSICAL CHEMISTRY A

ARTICLE

pubs.acs.org/JPCA

Pressure Induced Isostructural Metastable Phase Transition of Ammonium Nitrate

Alistair J. Davidson,[†] Raja, S. Chellappa,[‡] Dana M. Dattelbaum,[‡] and Choong-Shik Yoo*[,†]

[†]Institute for Shock Physics and Department of Chemistry, Washington State University, Pullman, Washington 99164-7041, United States

[‡]Shock and Detonation Physics, MS P952, Los Alamos National Laboratory, Los Alamos, New Mexico 87545, United States

Supporting Information

ABSTRACT: The energetic material ammonium nitrate (AN, NH_4NO_3) has been studied under both hydrostatic and nonhydrostatic conditions using diamond anvil cells combined with micro-Raman spectroscopy and synchrotron X-ray powder diffraction. The refined powder X-ray data indicates that under hydrostatic conditions AN-IV (orthorhombic, *Pmmn*) is stable to above 40 GPa. In *one* nonhydrostatic compression experiment a volume collapse was observed, suggesting an isostructural phase transition to a "metastable" phase IV′ between 17 and 28 GPa. The structures of phase IV and IV′ are similar with the subtle difference in the hydrogen-bonding network; that is, a noticeably shorter N1···O1 distance seen in phase IV′. This hydrogen bond has a significant component along the *b*-axis, which proves to be the most compressible until cell axis over the entire pressure range. It is likely that the shear stress of the nonhydrostatic experiment drives the phase IV-to-IV′ transition to occur. We compare the present isotherms of phase IV and IV′ in both static and nonhydrostatic conditions with the previously obtained Hugoniot and find that the nonhydrostatic isotherm approximately matches the Hugoniot. On the basis of this comparison, we conjecture that a chemical reaction or phase transition may occur in AN under dynamic pressure conditions at 22 GPa.

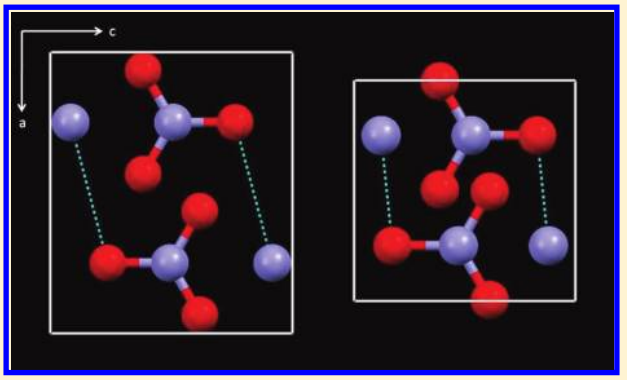

1. INTRODUCTION

High-pressure polymorphism and phase transitions have wide ranging consequences on the basic properties of molecular solids such as intermolecular interactions, chemical bonding, crystal structures, and thermoelastic properties. One class of materials upon which this has a considerable effect is that of energetic materials.[1,2] Two different polymorphs of the same energetic material, for example, often display significantly different properties and energetic performance attributes such as crystal density, detonation velocity, shock sensitivity, and detonation chemistry.[3,4] Importantly, phase transitions do occur over a large pressure−temperature range in relevance to chemical detonation (to 50 GPa and 4000 K),[5−7] which can alter energetic processes in a fundamental way.

There has been a high level of effort exerted in the aim of understanding and characterizing high pressure properties of energetic materials, such as shock Hugoniot and detonation velocities under dynamic conditions in terms of continuum measurements.[6,8] However, in comparison there have been relatively few studies investigating pressure-induced changes at the *molecular* level under static high pressures.[2,9] This constitutes a major shortcoming, considering the fact that nearly all molecular solids including most energetic materials exhibit a profound polymorphism under high pressures as they undergo major modifications in intermolecular interaction, typically starting at relatively low pressures of 1−10 GPa. In this regard, high-pressure structural studies are an excellent way of understanding and modeling not only the performance characteristics of energetic materials but also the exact nature of chemical bonding and pressure-induced changes that leads to chemical reactions such as detonation.

Ammonium nitrate (AN, NH_4NO_3) is a strong oxidizer commonly used as an agricultural fertilizer. When mixed with a few percent of hydrocarbons (or fuel oil), it becomes an explosive, often called ANFO, used in mining industries. Because of its wide availability as a fertilizer, chemical mixtures of AN have also been exploited in the construction of improvised explosive devices (IEDs). AN has also attained a significant amount of publicity due to numerous disasters occurring during transportation and storage (most notably the Texas City disaster in 1947).[10] Many of these accidents have occurred as a result of AN unintentionally catching fire, leading to large-scale explosions.[10] AN is marketed in several forms, depending on the

Received: August 12, 2011
Published: September 08, 2011

Table 1. Crystallographic Information for Phases I−V of AN

Phase	I	398 K	II	357 K	III	305 K	IV	255 K	V
Space group	$P4_2$		*Pmmn*		*Pnma*		*P4/mbm*		*Pm3m*
Crystal system	Cubic		Tetragonal		Orthorhombic		Orthorhombic		Tetragonal
a (Å)	4.37		5.696		7.716		5.751		7.997
b	4.37		5.696		5.845		5.436		7.997
c	4.37		4.920		7.197		4.926		9.830
Z	1		2		4		2		8

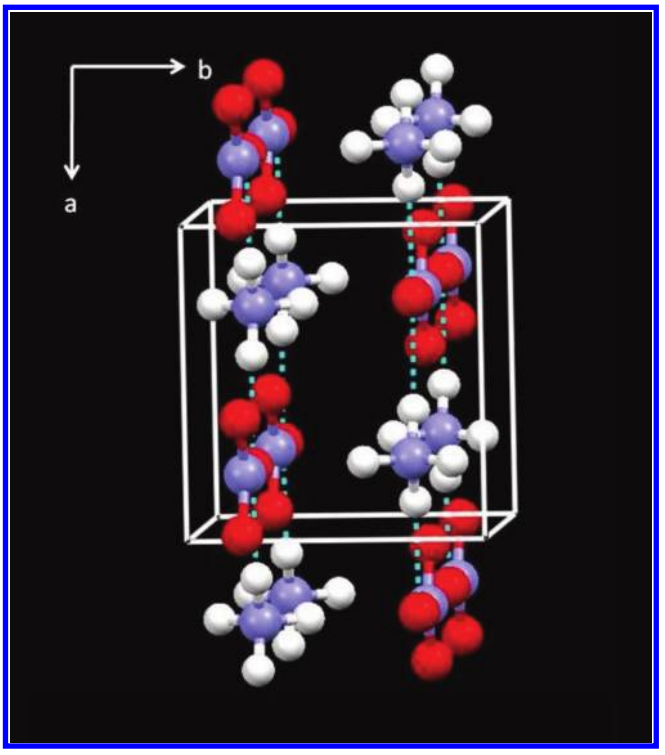

Figure 1. Extended crystal structure of phase IV of AN at ambient pressure, viewed down the *c*-axis, showing two-dimensional hydrogen bonded network (hydrogen bonds in blue).

use. Liquid AN is sometimes sold as a fertilizer, generally in combination with urea. Solid AN may be produced in the form of prills, grains, granules, or crystals. Prilled or granulated AN are often used in ANFO, as they can have increased porosity compared to other solid forms, which enables great absorption of fuel oil, leading to a high detonation velocity.[11]

Ammonium nitrate is an excellent example of an energetic material displaying rich polymorphism. Under ambient pressure, six known phases have been accessed at different temperatures. Five of these have been structurally characterized[12−16] (phases I−V), with a further phase VI being proposed at 103 K, but with no structural information reported.[17] Crystallographic data of phases I−V are summarized in Table 1.

Phase IV is stable at ambient conditions of temperature and pressure. The structure has been determined to be orthorhombic (*Pmmn*), with one ammonium ion, and one nitrate ion in the asymmetric unit. In this structure, AN molecules comprise a two-dimensional network of hydrogen bonding. This hydrogen-bonding network forms infinite sheets parallel to the (001) planes of the crystal, with adjacent sheets bound together by van der Waals forces (Figure 1). Phase III is also orthorhombic (*Pnma*), with four formula units per unit cell. The low temperature phase V is noncentric tetragonal, crystallizing in space group $P4_2$. Phase II, the high- temperature phase of AN, is also tetragonal (*P4/mbm*). Phase I has a CsCl type structure with $z = 1$ in a cubic unit cell (*Pm3m*).

Under high pressures, Bridgman was the first to recognize that AN did not undergo a phase transition under hydrostatic conditions below 5.0 GPa.[18] However, under nonhydrostatic conditions, two shear-induced transitions were reported at 0.45 and 2.7 GPa, on the basis of the pressure-induced changes in the Raman spectra.[19] More recently, hydrostatic X-ray diffraction experiments performed using a diamond-anvil cell (DAC) did not identify any evidence of a phase transition in the range 0−25 GPa.[20] It was stated that if any phase transition did occur, they would be subtle and retain a significant similarity to that of phase IV. The aim of the present study has been to investigate the phase behavior of AN in both hydrostatic and nonhydrostatic conditions using a combination of micro-Raman spectroscopy and powder X-ray diffraction and extend the definition of the room temperature isotherm to higher pressure.

2. EXPERIMENTAL SECTION

High pressures were generated using a membrane-diamond anvil cell (DAC), equipped with 300 μm culet diamonds and a rhenium gasket (hole size ca. 150 μm). Powdered samples of AN (the first batch provided by Sigma-Aldrich in 99.999% purity and the second batch by Los Alamos National Laboratory) were used in experiments, with either ruby chips[21] or powdered Au used for pressure determination. Experiments were conducted under both hydrostatic and nonhydrostatic conditions. Hydrostatic experiments were performed using helium as a pressure-transmitting medium, which was loaded using a Washington State University designed high-pressure gas-loading device. Nonhydrostatic experiments were performed in the absence of any pressure-transmitting medium for comparison.

High-pressure angle dispersive X-ray diffraction experiments were undertaken on beamline 16BMD (λ = 0.424 60 Å) and 16IDB (λ = 0.367 93 Å)/HPCAT equipped with an image plate (MAR 345) at the Advanced Photon Source (APS) in Argonne

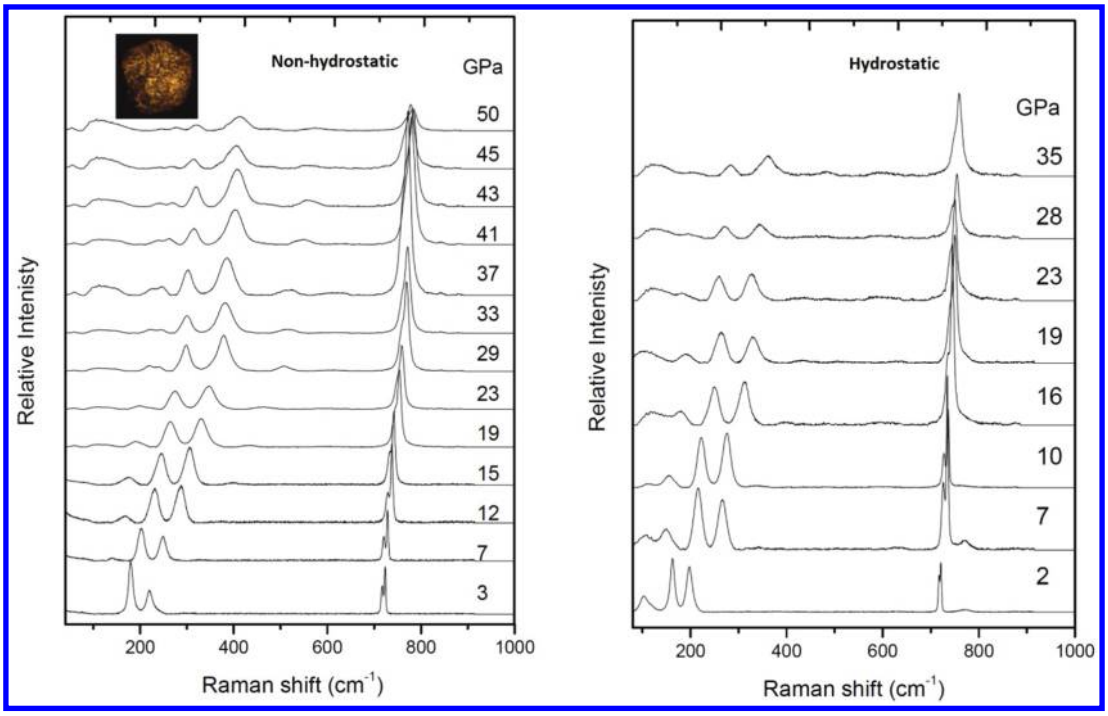

Figure 2. Raman spectrum of AN in (a) nonhydrostatic and (b) hydrostatic conditions as a function of pressure. Inset in (a) represents a visual image of AN loaded as a powder into a diamond anvil cell.

National Laboratory. The characteristics of the diffraction experiment were calibrated with a CeO_2 standard with a microfocused X-ray beam of ~10 × 20 μm full width at half-maximum on 16 BMD and ~7 × 6 μm at 16 IDB, which typically provides high-pressure diffraction patterns free from scattering from the gasket. All diffraction experiments were conducted at room temperature. X-ray diffraction intensities were integrated using the program FIT2D. Rietveld and LeBail refinements were performed for all powder patterns using the General Structure Analysis Software (GSAS) suite of programs.[22]

All Raman spectra were collected in a backscattering geometry using an in-house confocal micro-Raman system employing an Ar^+ laser of 514.5 nm.

3. RESULTS AND DISCUSSION

3.1. Raman Spectroscopy. Ammonium nitrate has been subject to several Raman spectroscopy studies in the past.[23,24] A factor group analysis of phase VI (D_{2h},[13] $z = 2$) predicts 27 Raman active modes distributed in $9A_g$, $8B_{1g}$, $7B_{2g}$, and $3B_{3g}$; the most external (rotational and translational) modes are below 250 cm^{-1} and the internal modes are above 700 cm^{-1}. Our Raman spectra collected at ambient pressure were in excellent agreement with those published spectra.[23,24] Of particular interest to this study was the low frequency region (100−1000 cm^{-1}). Raman spectra were collected at incremental pressure steps between 0.5 and 5.0 GPa under nonhydrostatic conditions (Figure 2a). Intense bands were observed under ambient conditions at 150 and 180 cm^{-1}. These peaks are associated with the rotational modes of the nitrate ion (respectively, B_{2g} and B_{3g} modes). A doublet was also observed at 715 cm^{-1}, which was due to the Davydov (or factor group) splitting of the internal normal mode ν_4 of the nitrate ion (A_g, B_{1g}). All observed peaks were seen to shift to higher wavenumbers with increasing pressure. Inspection of the collected Raman spectra revealed the appearance of a new vibrational band at ca. 390 cm^{-1} between 15 and 19 GPa. It is believed that this new peak is associated with the rotational lattice modes of the NO_3^{-1} ion, suggesting a possible phase transition occurring at this pressure, possibly arising from a change in the hydrogen-bonding network. The experiment was repeated under hydrostatic conditions using a He pressure medium, with no significant changes in the vibrational bands seen up to a pressure of 35 GPa (Figure 2b). Furthermore, inspection of the Raman shifts of each peak with increasing pressure did not reveal any discontinuities. This experiment was repeated, with the same result obtained each time.

3.2. X-ray Powder Diffraction: Hydrostatic Studies. X-ray powder diffraction patterns were collected under hydrostatic conditions at incremental pressure steps to 20 GPa on a powdered sample of AN (Sigma-Aldrich). Indexing of the observed peaks identified the presence of the orthorhombic (*Pmmn*) phase IV of AN, with the observed lattice parameters demonstrating good agreement with previous studies[20,25] (a = 5.5528(18), b = 4.9322(18), and c = 4.7301(13) Å).

Full-profile Rietveld refinements of the diffraction patterns enabled refinement of the crystal structures up to 20 GPa (Figure 3). Phase IV was shown to persist to the highest pressure of this study. Changes were observed in the N···O−N distances in the two-dimensional hydrogen bonded network, which decreased by 0.1−0.4 Å over the entire pressure set. The largest change was observed in the N1···O1 distance. The van der Waals distances between the hydrogen bonded sheets decreased by 0.5 Å over the pressure range. All lattice parameters were seen to decrease with increasing pressure, with the b-axis proving to be the most compressible, decreasing by approximately 20% by the final pressure point (Figure 4). The a-axis and c-axis decrease by 12% and 9%, respectively. This was in agreement with previous

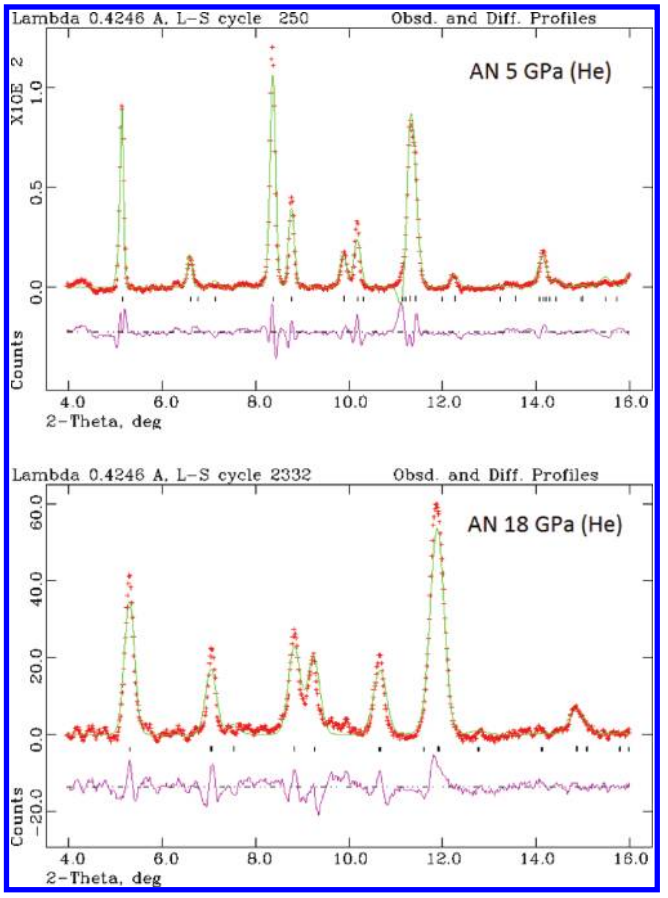

Figure 3. X-ray powder diffraction patterns of AN in hydrostatic pressures of 5 and 18 GPa. The crosses denote the observed intensities and the solid lines those calculated from the best-fit model of the Rietveld refinement. The tic marks represent the calculated peak positions. The line below them represents the difference between observed and calculated intensities.

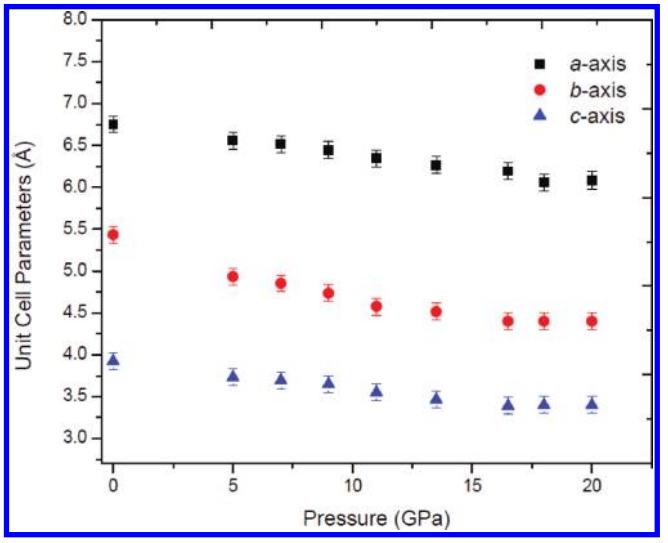

Figure 4. Lattice parameters of phase IV of AN under hydrostatic conditions (He) as a function of pressure.

studies.[20,25] The decrease in lattice parameters by 20 GPa led to a net decrease in the unit cell volume of 35%, as shown in Figure 5.

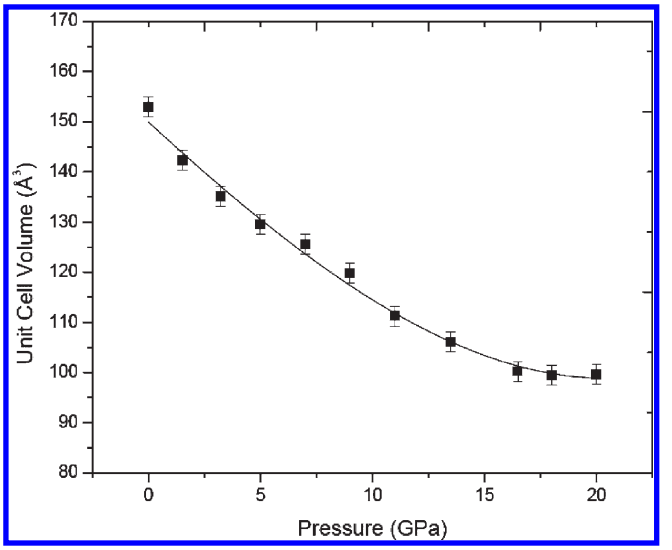

Figure 5. Pressure−volume compression curve of phase IV of AN determined under hydrostatic conditions using He as a pressure medium.

The hydrogen bonding distance N1···O1 has a significant component along the *b*-axis and could explain why this axis is the most compressible. The change in the variation of the unit cell volume with increasing pressure could be fitted to a third-order Birch−Murnaghan plot with V_o = 153.89 Å^3, B_o = 10.69(10) GPa, and B_0' = 7.7. The values of V_o and B_0' were fixed for comparison with previous data. The values differ slightly from the previous known equation of state.[20,25] However, previous hydrostatic high-pressure experiments were conducted using either nitrogen or a methanol/ethanol mixture, as pressure transmitting media. These experiments could be assumed to be close to nonhydrostatic with respect to the hydrostatic condition provided by helium above 10 GPa, and thus could explain the discrepancies between the values.

3.3. Powder X-ray Diffraction: Nonhydrostatic Studies. X-ray powder diffraction patterns were collected to 35 GPa on a ground powdered sample of AN (Sigma-Alrich). Initial indexing at 7 GPa confirmed the presence of phase IV with the lattice parameters of a = 5.5073(24), b = 4.8853(19), and c = 4.7240(31) Å. Full-profile Rietveld refinements were possible up to 17 GPa, with phase IV again remaining present (Figure 6). Similar changes to the hydrostatic experiments in the hydrogen bonding network were observed, with the N···O−N and Van der Waal distances decreasing by 0.2−0.3 and 0.4 Å, respectively. A decrease in the unit cell parameters was observed, with the *b*-axis again proving to be the most compressible (Figure 7). The *a*-, *b*-, and *c*-axis decrease by 7%, 15%, and 6%, respectively. A decrease of 25% was observed in the unit cell volume between 0 and 17 GPa. The smooth variation in volume could be fitted to a third-order Birch−Murnaghan plot with V_o = 153.92(2) Å^3, B_o = 15.37(14) GPa, and B' = 9.8(30). These values were in good agreement with previous studies (B_0 = 16.6(7) GPa and B' = 7.7(4)[25]).

At 21 GPa, a visual change was seen in the Debye−Scherrer diffraction rings, with a marked decrease in intensity observed in the integrated powder pattern (Figure 6). This new powder pattern could be indexed to a new orthorhombic system with the space group *Pmmn*, (isostructural to phase IV) with lattice parameters a = 5.145(2), b = 4.508(5), and c = 4.502(2) Å. This new phase is denoted here as phase IV′ of AN. This phase

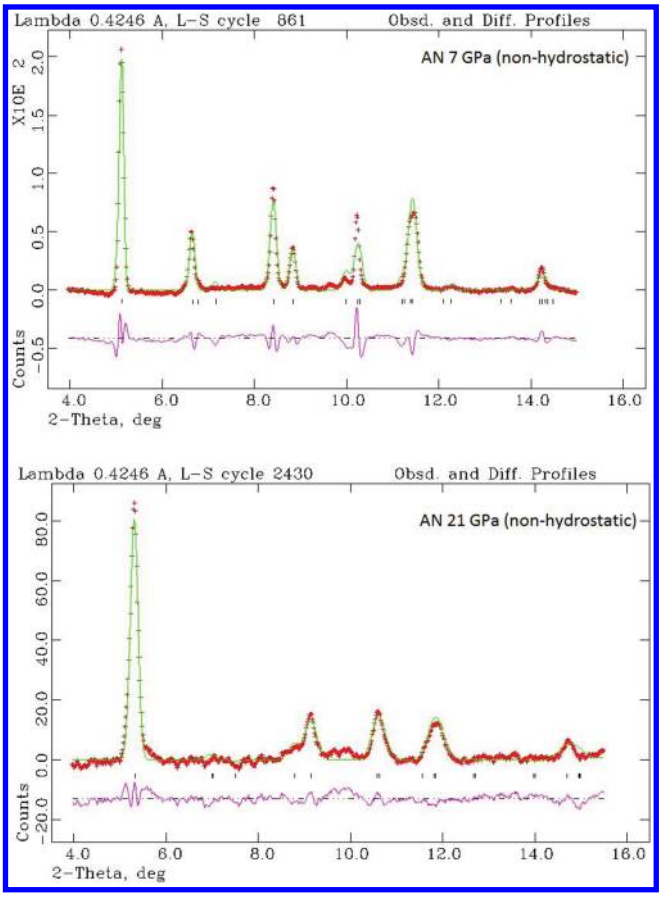

Figure 6. X-ray powder diffraction pattern of AN (nonhydrostatic) at 7 and 21 GPa, respectively. The crosses denote the observed intensities and the solid lines those calculated from the best-fit model of the Rietveld refinement. The tic marks represent the calculated peak positions. The line below them represents the deviation between observed and calculated intensities.

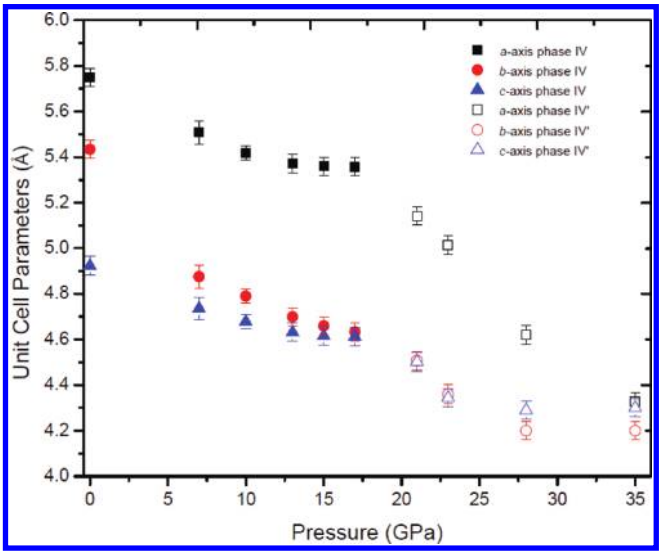

Figure 7. Evolution of lattice parameters of phase IV and IV′ with increasing pressure under nonhydrostatic conditions.

persisted to 35 GPa, the maximum pressure of the present study. Subsequent Rietveld refinement was possible by inserting the known atomic positions for phase IV of AN, and refining initially with heavy damping and appropriate soft constraints. All damping was removed by final refinement. It was possible to refine all subsequent powder patterns up to 35 GPa in the context of the crystal structure of phase IV′ reasonably well, with typical χ^2 values of 0.29 and wR_p = 0.026. Inspection of the crystal structure at 21 GPa did not show any marked changes, indicating, as expected, that this was a subtle transformation. The response of all three lattice vectors for both phase IV and phase IV′ are displayed in Figure 7. Across the phase IV−IV′ transition between 17 and 25 GPa, all three axes decreased, which led to a net decrease in the unit cell volume of 9%. The associated increase in density over the transition was from 2.32 to 2.54 g/cm^3. Further inspection of the crystal structure at 28 GPa did, however, reveal some interesting changes. It can be seen that the NO_3 groups shift along the (101) plane to facilitate the formation of a favorable O1···N1 contact. This bond decreased by 0.1 Å over the transition. A decrease was also seen in the van der Waals distances between the hydrogen bonded sheets of 0.07 Å. This can be seen in Figure 8. It is likely that the formation of this favorable shorter hydrogen bonding in the denser phase IV′ could be the driving force behind this transition. Inspection of the crystal structure above 17 GPa indicates that this transition is sluggish, most likely occurring between 17 and 28 GPa.

On slow decompression, the new phase IV′ was seen to persist to 0.1 GPa, based on its Raman and X-ray diffraction characteristics. However, on pressure release, the resulting powder pattern confirmed that a transformation had occurred back to phase IV. This indicates that phase IV′ is thermodynamically unstable under ambient pressure conditions, and likely to be a metastable phase. In addition, the fact that the transition was reversible also seems to rule out any possible decomposition or chemical reactions occurring at high pressure. The change in the variation of the unit cell volume of phase IV′ with decreasing pressure could be fitted to a third-order Birch−Murnaghan plot with V_o = 126.2(8) Å^3, B_o = 22.7(7) GPa, and B' = 6.3(4).

To confirm this phase transition, nonhydrostatic compression of AN was repeated up to 24 and 40 GPa on powdered crystalline AN samples. Lebail refinements showed that phase IV of AN persisted up to 40 GPa with no evidence of transition to phase IV′. This further backs up the suggestion that phase IV′ of AN seen in the first nonhydrostatic experiment is most likely to be a metastable phase.

A further point to note is that the transition pressure observed in the X-ray experiments is different from that seen in the Raman experiment. This could be due to the fact that the local symmetry of AN changes at 15 GPa (as seen in the Raman spectra), but that a phase transition does not occur until a slightly higher pressure (as seen in X-ray experiments).

4. DISCUSSION

The most striking result of the present work is the different compression behavior of AN depending on the hydrostaticity. Figure 9 plots the pressure−volume compression curves obtained in hydrostatic and nonhydrostatic conditions in the present study, together with previous results.[20,25,26] The present data are in excellent agreement with the previous experiments in the range 0−10 GPa. However, above 10 GPa, different behavior can be observed depending on the hydrostaticity of the sample. The differences in hydrostaticity can be explained by considering

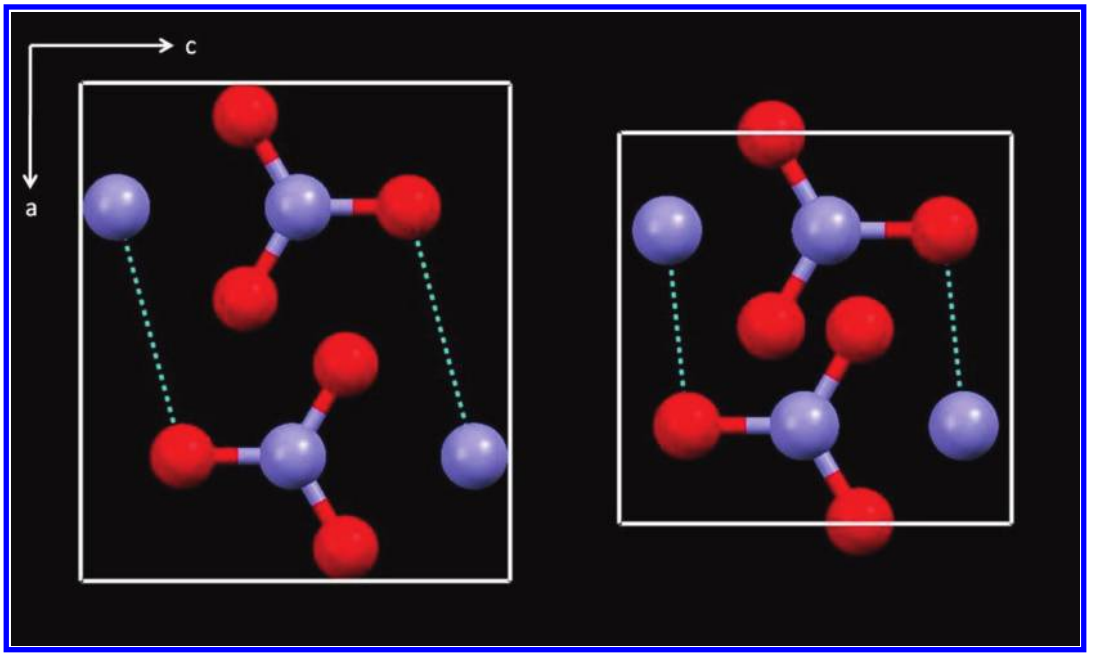

Figure 8. Crystal structures of AN at (a) 15 GPa (b) 28 GPa viewed down the *b*-axis. Nitrogen and oxygen atoms are shown in blue and red balls, respectively, whereas, hydrogen atoms are not shown for clarity. The hydrogen-bonding network is signified by the dotted line between nitrogen and oxygen atoms.

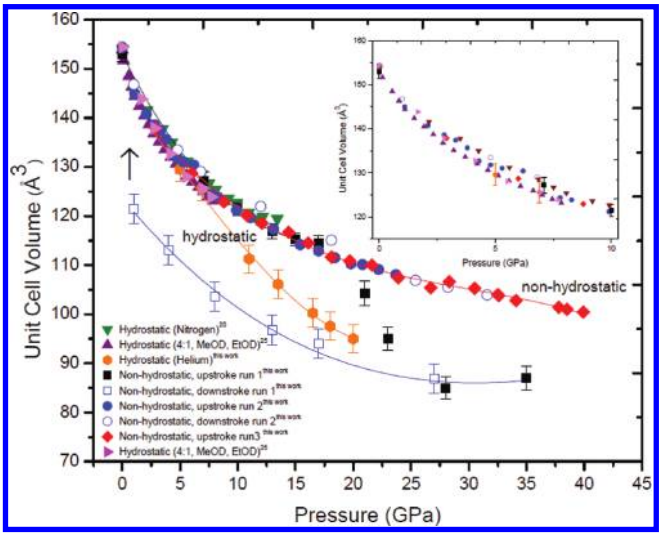

Figure 9. Pressure−volume relationship of AN under hydrostatic and nonhydrostatic conditions, plotted together with previous results from X-ray and neutron diffraction experiments.

that the previous hydrostatic work was conducted using nitrogen as a pressure-transmitting medium. As such, helium is considered a more hydrostatic pressure-transmitting medium above 10 GPa than nitrogen. This explanation is further supported by the fact that our nonhydrostatic data show significant similarity to the work conducted both with nitrogen as a pressure transmitting medium and in previous nonhydrostatic experiments.

It is interesting to note in Figure 9 that the pressure−volume compression behavior of AN in nonhydrostatic condition is initially stiffer than in hydrostatic conditions but becomes substantially softer above ~15 GPa. In most cases, the deviatoric stress in nonhydrostatic conditions should stiffen the compression curve, as observed below 15 GPa. The observed softening of the compression curve at higher pressures (solid squares) can then be attributed to the fact that the IV−IV′ phase transition occurs over a broad pressure range under nonhydrostatic conditions, between 17 and 28 GPa. Sluggish behavior coupled with large hysteresis is typical of a shear-induced phase transition and is often described as a second-order phase transition. In fact, the compression behavior of the high-pressure phase IV′ (open squares) shows a compression behavior similar to that of the low-pressure phase IV. A similar softening effect on the compression curve in nonhydrostatic conditions has been previously observed in the high-explosive HMX,[27] but this was reported to be due to a shear-induced chemical reaction.

The other notable result in this work is the fact that we only observe the formation of phase IV′ of AN in the first nonhydrostatic experiment. This is of significant interest and sheds light on the different behavior between the hydrostatic and nonhydrostatic data. Inspection of Figure 9 shows that the volume−pressure relationship of phase IV′ tends toward the hydrostatic behavior of phase IV at higher pressures, i.e., acting as a bridge between the hydrostatic and nonhydrostatic states, suggesting that phase IV′ of AN could be a metastable state. This observation is further supported by the extended stability of phase IV′ on decompression.

The fact that phase IV′ has been observed *only once* under nonhydrostatic conditions is not unusual. There are numerous examples in the literature that describe the formation of "elusive polymorphs", where reproducibility of a new polymorph has been extremely difficult to achieve.[28] For example, a possible reason for the differences between data sets could be a result of AN's ability to absorb moisture from the air. In case of AN, the presence of moisture is known to result in temperature-induced transition to a metastable phase (i.e., phase III of AN). The first batch of AN was loaded directly as provided by Sigma-Aldrich. The second and third batched were baked/dried to remove

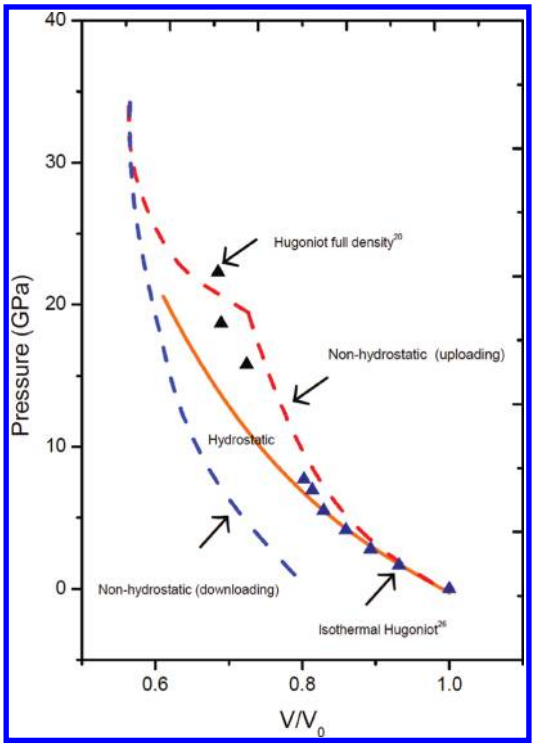

Figure 10. Isotherms of AN in comparison with the Hugoniot of shock-compressed AN powder, showing the similarity between the nonhydrostatic isotherm and the Hugoniot. Black triangles refer to previous shock Hugoniot; blue triangles to a previous isothermal Hugoniot.

moisture (the sample was evacuated in an oven at 40−45 °C overnight to remove any moisture). The different behavior could thus possibly be attributed to the different solid form of AN used in each of the studies. It may be that two different powdered samples used in our experiments, could explain the differences. For example, it may be possible that phase IV′ would be seen in experiments conducted on other forms of AN at higher pressures.

A shear-induced phase transition of AN in nonhydrostatic conditions is interesting and in agreement with recent studies that did not identify any phase transitions in phase IV under hydrostatic conditions. It can be assumed that the stability of AN under these conditions is a result of the stable hydrogen bonding network. Previous work has suggested that any transformations in AN would be very subtle, with only small changes in the structure observed. Previous studies had also inferred that AN was most likely to undergo a phase transition under nonhydrostatic conditions. Both these suggestions proved to be correct. It appears that the application of shear stress causes changes to occur in the crystal structure of AN, which manifest themselves in the formation of a favorable hydrogen bond. This behavior is not unprecedented. There are occasions when nonhydrostatic behavior has caused shear stresses which induced phase transitions, such as reported for silver nitrate.[19]

5. COMPARISON WITH SHOCK WAVE DATA

Figure 10 compares our isotherms collected under hydrostatic (orange line of best fit) and nonhydrostatic (red line of best fit) conditions with the shock Hugoniot data of unreacted AN (black[20] and blue[26] triangles). Clearly, we find that the Hugoniot data shows more similarities with the nonhydrostatic isotherm. This is as expected, as shock wave compression is completely nonhydrostatic in nature. A close inspection of the Hugoniot data also reveals a subtle yet notable difference between the nonhydrostatic isotherm and the Hugoniot. Previous shock wave profiles that exhibit no apparent sign for a phase transition (or chemical reaction) such as a two-wave structure. As such, a plausible explanation for this discrepancy may be a kinetic effect associated with the shear-induced phase transition: shock loading typically occurs within a few 100 ns, perhaps not long enough to induce a phase transition in AN. Nevertheless, note that the Hugoniot point at 22 GPa does not quite fit with other Hugoniot points, which could possibly indicate the onset of a phase transition or, more likely, a chemical reaction to an expanded state.

Pressure-induced phase transitions and chemical changes in energetic materials originate from compressed states, regardless of static or shock conditions. This occurs when the compression energy ($P\Delta V$) exceeds or rivals the stability of the ambient phase, written explicitly in the lattice and chemical bond energies. The difference in the final states is due to the different reaction pathways; the statically induced reaction in a confined volume leads to a denser final state, whereas the shock-induced reaction results in an open expanded state of simple molecular mixtures. Interestingly, pressure-induced phase transitions observed at static pressures of 27 GPa for HMX,[27] 7.5 GPa for nitromethane,[29] and 13 GPa for hydrogen peroxide[30] occur within 20% of the detonation pressures of 30, 12, and 13 GPa, respectively.

6. CONCLUSIONS

In conclusion, ammonium nitrate has been studied under conditions of both hydrostatic and nonhydrostatic pressure using both Raman spectroscopy and powder X-ray diffraction. We present a single observation of a possible shear-induced phase transition to new metastable phase IV′ in nonhydrostatic conditions over a broad pressure range of 17−28 GPa. The structure of phase IV′ has characterized to be isostructural to phase IV with the main structural difference in the hydrogen-bond networks. We also report that no phase transition was observed in AN up to 35 GPa under hydrostatic conditions. This information is crucial not only for understanding polymorphism in AN but also in other energetic and explosive materials. The new compression data of AN phases presented in this paper will be extremely useful in theoretical modeling of detonation in AN-based materials.

■ ASSOCIATED CONTENT

Supporting Information. Crystallographic information files for phase IV′ of AN at 28 GPa. This material is available free of charge via the Internet at http://pubs.acs.org.

■ AUTHOR INFORMATION

Corresponding Author
*E-mail: csyoo@wsu.edu.

■ ACKNOWLEDGMENT

We thank the CDAC for the provision of X-ray beamtime 16 BDM and 16 IDB, and Dmitry Popov and Stas Sinogeikin for their assistance during the experiments. The present study has been supported by the U.S. Department of Homeland Security

under Award Number 2008-ST-061-ED0001 and NSF-DMR (Grant No. 0854618). The views and conclusions contained in this document are those of the authors and should not be interpreted as necessarily representing the official policies, either expressed or implied, of the U.S. Department of Homeland Security.

REFERENCES

(1) Oswald, I. D. H.; Millar, D. I. A.; Davidson, A. J.; Francis, D. J.; Marshall, W. G.; Pulham., C. R.; Cumming, A. S.; Lennie, A. R; Warren, J. E. *High Pressure Res.* **2010**, *30* (2), 280–291.

(2) Davidson, A. J.; Oswald, I. D. H.; Francis, D. J.; Lennie, A. R.; Marshall, W. G.; Millar, D. I. A.; Pulham, C. R.; Warren, J. E.; Cumming, A. S. *CrystEngComm.* **2008**, *10*, 162–165.

(3) Akhavan, J. *The Chemistry of Explosives*; Royal Society of Chemistry, 2nd ed.; Cambridge, U.K., 2004.

(4) Fabbiani, F. P. A.; Pulham, C. R. *Chem. Soc. Rev.* **2006**, *35*, 932–942.

(5) Zel'dovich, Y. B.; Raiser, Y. P. *Physics of Shockwaves and High Temperature Hydrodynamics Phenomena*; Academic Press: New York, 1966.

(6) Shaw, R. W.; Brill, T. B.; Thompson, D. L. *Overview of Recent Research on Energetic Materials, Advanced Series in Physical Chemistry*; World Scientific: Singapore, 2005; p 16.

(7) Brill, T. B. Polymorphism and Phase Transformations in Energetic Materials, 35th Course; International School of Crystallography: Erice, Italy, 2004.

(8) Barton, A. F. M.; Hodder, A. P. W. *Chem. Rev.* **1973**, *73* (2), 127–139.

(9) Peiris, S. M.; Pangilinan, G. I.; Russell, T. P.; Westrum, E. F., Jr.; Justice, B. H. *J. Phys. Chem. A* **2000**, *104*, 1118.

(10) Stephens, H. W. *The Texas City disaster, 1947*; University of Texas Press: Austin, TX, 1997.

(11) Zygmunt, B.; Buczkowski, D. *Propellants, Explos., Pyrotech.* **2007**, *32*, 411–414.

(12) Amoros, J. L.; Arrese, F.; Canut, M. *Z. Kristallogr.* **1962**, *117*, 92–107.

(13) Choi, C. S.; Mapes, J. E.; Prince, E *Acta Crystallogr.* **1972**, *B28*, 1357–1361.

(14) Hendricks, S. B.; Posnjak, E.; Kracek, F. C. *J. Am. Chem. Soc.* **1932**, *54*, 2766–2786.

(15) Holden, J. R.; Dickinson, C. W. *J. Phys. Chem.* **1975**, *79*, 249–256.

(16) Lucas, B. W.; Ahtee, M.; Hewat, A. W. *Acta Crystallogr.* **1979**, *B35*, 1038–1041.

(17) Choi, C. S.; Prask, H. J. *J. Appl. Crystallogr.* **1980**, *13*, 403–409.

(18) Bridgman, P. W. *Proc. Am. Acad. Arts Sci.* **1937**, *71*, 387.

(19) Adams, D. M.; Sharma, K. A. *J . Chem. Soc., Faraday Trans. 2* **1981**, *77*, 1263–1272.

(20) Robbins, D. L.; Sheffield, S. A.; Dattelbaum, D. M.; Velisavljevic, N.; Stahl, D. B. *Shock Compression Condens. Matter—1991, Proc. Am. Phys. Soc. Top. Conf., 7th* **2009**, 552–555.

(21) Piermarini, G. J.; Block, S.; Barnett, J. D.; Forman, R. A. *J. Appl. Phys.* **1975**, *46*, 2774–2780.

(22) Larson, A. C.; Von Dreele, R. B. *Los Alamos National Laboratory Report No. LA-UR-86-748*; Los Alamos National Laboratory: Los Alamos, NM, 1987.

(23) Kearley, G. J.; Kettle, F. A. *J. Chem. Phys.* **1980**, *73* (5), 2129–2136.

(24) Akiyma, K.; Morioka, Y.; Nakagawa, I. *Bull. Chem. Soc. Jpn.* **1981**, *54*, 1662–1666.

(25) Davidson A. J. *Ph.D. thesis*, University of Edinburgh, 2004.

(26) Sandstrom, F. W. *Ph.D. thesis*, New Mexico Institute of Mining and Technology in Socorro, Socorro, NM, 1994.

(27) Yoo, C.-S.; Cynn, H. *J. Chem. Phys.* **1999**, *111*, 10229–10235.

(28) Oswald, I. D. H.; Chataigner, I.; Elphick, S.; Fabbiani, F. P. A.; Lennie, A. R.; Maddaluno, J.; Marshall, W. G.; Prior, T. J.; Pulham, C. R.; Smith, R. I. *CrystEngComm.* **2009**, *11*, 359–366.

(29) Courtecuisse, S.; Cansell, F.; Fabre, D.; Petitet, J.-P. *J. Chem. Phys.* **1995**, *102* (2), 968–974.

(30) Chen, J.-Y.; Kim, M.; Yoo, C.-S.; Dattelbaum, D. M.; Sheffield, S. *J. Chem. Phys.* **2010**, *132*, 214501–124507.